

Research



Cite this article: Araujo RM, Valerio MEG, Jackson RA. 2014 Computer simulation of metal co-doping in lithium niobate. *Proc. R. Soc. A* **470**: 20140406.
<http://dx.doi.org/10.1098/rspa.2014.0406>

Received: 21 May 2014

Accepted: 4 August 2014

Subject Areas:

computational chemistry, solid-state physics

Keywords:

lithium niobate, co-doping, computer modelling

Author for correspondence:

Robert A. Jackson

e-mail: r.a.jackson@keele.ac.uk

One contribution to a Special feature 'New developments in the chemistry and physics of defects in solids'.

Computer simulation of metal co-doping in lithium niobate

Romel M. Araujo¹, Mário E. G. Valerio² and Robert A. Jackson³

¹Chemistry Department, Pio Decimo College, Campus III, 49095-000 Aracaju, SE, Brazil

²Physics Department, Federal University of Sergipe, 49100-000 São Cristóvão, SE, Brazil

³School of Physical and Geographical Sciences, Keele University, Keele ST5 5BG, UK

 RAJ, 0000-0002-1163-6421

Lithium niobate, LiNbO_3 , is an important technological material with good electro-optic, acousto-optic, elasto-optic, piezoelectric and nonlinear properties. Computer modelling provides a useful means of determining the properties of the material, including its defect chemistry, and the effect of doping on the structure. In this work, double-doped LiNbO_3 was studied, and the energetics of the solid-state reactions leading to incorporation of the dopants was calculated. The following combinations of dopants were studied: Fe and Cu; Ce and Cu; Ce and Mn; Fe and Rh; and Ru and Fe. For most of these combinations, the co-doping process decreases the energy required for incorporation of the dopants, and the final defect configurations are consistent with experimental results, where available.

1. Introduction

Lithium niobate, LiNbO_3 , is a material of great technological importance, with many applications in devices that exploit its properties, which range from elastic to photorefractive [1–4].

LiNbO_3 crystals have been extensively investigated as holographic recording materials because of their attractive photorefractive properties, and their availability in large size and good quality [5]. Experimental results show that non-volatile holographic recording has been achieved in LiNbO_3 crystals with the following combinations of dopants: Fe, Cu; Ce, Cu; Ce, Mn; Fe, Rh; and Ru, Fe. In addition, LiNbO_3 :

Table 1. Dopant–oxygen potentials obtained by fitting to parent oxide structures.

interaction	A_{ij} (eV)	ρ_{ij} (Å)	C_{ij} (eVÅ ⁶)
Fe ³⁺ –O ²⁻	1438.60	0.3148	3.58
Ce ⁴⁺ –O ²⁻	1965.72	0.3496	14.38
Ce ³⁺ –O ²⁻	2803.18	0.3289	27.55
Cu ⁺ –O ²⁻	1328.98	0.2576	0.0
Mn ²⁺ –O ²⁻	722.30	0.2997	0.0
Rh ³⁺ –O ²⁻	1498.56	0.3298	0.0
Ru ⁴⁺ –O ²⁻	1324.89	0.3429	0.0

Zn, Fe was found to have improved holographic properties compared with crystals of LiNbO₃: Fe [6]. A comprehensive study by McMillen *et al.* [7] showed that ability to record a hologram, the stability of the system and the scattering of light are all strongly influenced by co-doping in LiNbO₃.

Computer modelling provides a useful means of determining the properties of materials, including their defect chemistry and the effect of doping on structure. Previous papers have presented a new potential model for LiNbO₃ [8] and reported the doping of structure by rare earth ions [9] and a range of trivalent ions [10]. This paper reports a computational study of the double doping of LiNbO₃ by Fe and Cu, Ce and Cu, Ce and Mn, Fe and Rh, and Ru and Fe. Solution energies are calculated for doping with these ions, which enable predictions of mechanisms of incorporation of the dopants to be made, and also help interpretation of the holographic recording properties of the material.

2. Methodology

(a) Modelling the perfect lattice structures

All materials are modelled using interatomic potentials of Buckingham form, supplemented by a Coulombic interaction term

$$V(r) = A \exp\left(\frac{-r}{r}\right) - Cr^{-6} + \frac{q_1q_2}{r}$$

In this equation, A , ρ and C are parameters whose values are obtained by empirical fitting, and q_1 , q_2 are the charges on the interacting ions. Full details of the derivation of the potential for LiNbO₃ are given in [8].

The additional potentials required for this study, representing the interactions between the dopant ions and oxygen, were obtained in a similar way, by fitting parameters to the parent oxide structures. The potential parameters are given in table 1, and table 2 summarizes the expected good agreement between experimental and calculated structures.

(b) Defect calculations: defect formation and solution energies

The defect calculations employed in this work use the Mott–Littleton approach [11] in which point defects are considered to be at the centre of a region where all interactions are treated explicitly, whereas approximate methods are employed for regions of the lattice more distant from the defect. The calculations were performed using the GULP code [12].

Defect formation energies, corresponding to doping ions into the LiNbO₃ lattice, are calculated, but, on their own, they do not include all the energy terms involved in defect formation. Hence, solution energies are calculated that also take into account formation of dopant

Table 2. Comparison of calculated and experimental lattice parameters.

oxide	structural reference		exp. lattice parameter (Å)	calc. lattice parameter (Å)	percentage difference
Fe ₂ O ₃	[13]	a = b = c	9.3930	9.3930	0.00
CeO ₂	[14]	a = b = c	5.4100	5.4100	0.00
Ce ₂ O ₃	[15]	a = b = c	11.4100	11.4100	0.00
Cu ₂ O	[16]	a = b = c	4.2685	4.2685	0.00
MnO	[17]	a = b = c	4.4510	4.4510	0.00
Rh ₂ O ₃	[18]	a	5.1590	5.1587	−0.01
		b	5.3810	5.2506	−2.42
		c	7.2410	7.4450	2.82
RuO ₂	[19]	a = b	4.4923	4.4486	−0.97
		c	3.0995	3.1723	2.35

ions from their parent oxides, and the formation of any charge compensation defects involved. For example, considering doping of a Cu⁺ ion at a Li⁺ site in LiNbO₃, and assuming that the following process occurs:



The energy of this reaction, E_{sol} , expressed per single dopant ion, is

$$E_{\text{sol}} = \frac{-1}{2}E_{\text{latt}}(\text{Cu}_2\text{O}) + E(\text{Cu}_{\text{Li}}) + E_{\text{latt}}(\text{Li}_2\text{O}).$$

In this equation, the ' E_{latt} ' terms are lattice energies, and $E(\text{Cu}_{\text{Li}})$ is the defect formation energy for Cu at a Li site. In §3, solution energies are reported for double doping in LiNbO₃. Basic defect formation energies, and lattice energies needed in these calculations, are given in table 3. Kröger–Vink [20] notation has been employed for the defects in table 3.

3. Results and discussion

Four different combinations of two dopants were considered in this paper: (i) two trivalent ions, (ii) one trivalent and one monovalent ion, (iii) one tetravalent and one divalent ion, and (iv) one tetravalent and one trivalent ion. These combinations were chosen because they are quoted in experimental work reported in the literature, and these combinations seem to give the best set of properties that enable new applications. The ions involved in these four combinations are Cu⁺, Mn²⁺, Rh³⁺, Fe³⁺ and Ce⁴⁺.

For each of the four possibilities, a series of mechanisms were devised including different charge compensation defects. All mechanisms were written as solid-state reactions and for each of them the solution energy (E_{S}) was calculated. The reactions are shown in the following sections, where Kröger–Vink [20] notation has been used.

(a) Two trivalent dopant ions ($M = \text{Rh}^{3+}$, $R = \text{Fe}^{3+}$)

1. Substitution of $M = \text{Rh}^{3+}$ and $R = \text{Fe}^{3+}$ at Li⁺ sites with lithium vacancy compensation:

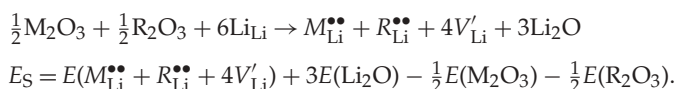
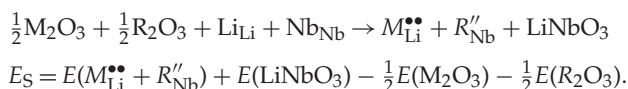


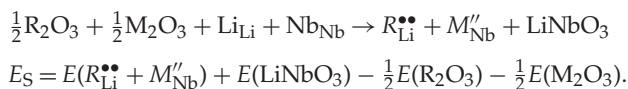
Table 3. Basic defect formation energies and lattice energies.

	0 K	293 K
<i>(a) basic defect formation energies per defect (eV)</i>		
V'_{Li}	9.81	9.71
V''''_{Nb}	127.56	127.45
$V^{\bullet\bullet}_0$	18.98	18.91
Li^{\bullet}	-7.08	-7.12
$\text{Nb}_i^{\bullet\bullet\bullet\bullet}$	-104.12	-104.25
O''_i	-9.47	-9.64
$\text{Nb}_{\text{Li}}^{\bullet\bullet\bullet\bullet}$	-98.37	-98.49
<i>(b) lattice energies (eV)</i>		
LiNbO_3	-174.57	-174.66
Li_2O	-33.16	-32.92
Nb_2O_5	-314.37	-313.99
CeO_2	-124.70	-124.77
Ce_2O_3	-129.32	-129.16
Fe_2O_3	-151.55	-151.63
Rh_2O_3	-118.16	-118.22
RuO_2	-115.64	-115.68
MnO	-38.32	-38.28
Cu_2O	-28.69	-29.81

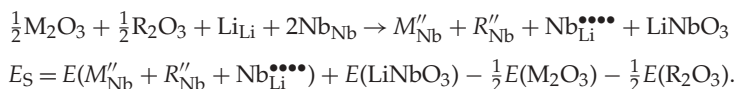
2. Self-compensation with $M = \text{Rh}^{3+}$ at a Li^+ site and $R = \text{Fe}^{3+}$ at a Nb^{5+} site:



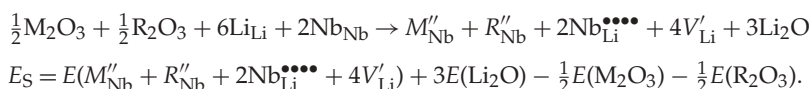
3. Self-compensation with $R = \text{Fe}^{3+}$ at a Li^+ site and $M = \text{Rh}^{3+}$ at a Nb^{5+} site:



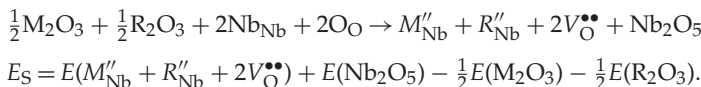
4. Substitution of $M = \text{Rh}^{3+}$ and $R = \text{Fe}^{3+}$ at Nb^{5+} sites with Nb^{5+} anti-site compensation:



5. Substitution of $M = \text{Rh}^{3+}$ and $R = \text{Fe}^{3+}$ at Nb^{5+} sites with compensation provided by a Nb^{5+} anti-site and a Li^+ vacancy:

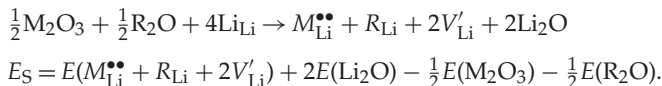


6. Substitution of $M = \text{Rh}^{3+}$ and $R = \text{Fe}^{3+}$ at Nb^{5+} sites with compensation given by an O^{2-} vacancy:

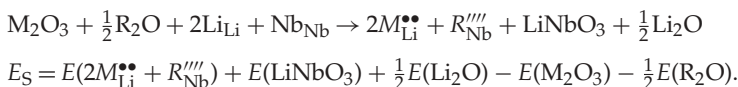


(b) One trivalent and one monovalent dopant ion ($M = \text{Ce}^{3+}$ or Fe^{3+} , $R = \text{Cu}^+$)

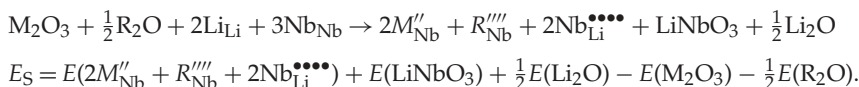
1. Substitution of $M = \text{Ce}^{3+}$, Fe^{3+} and $R = \text{Cu}^+$ at Li^+ sites with Li^+ vacancy compensation:



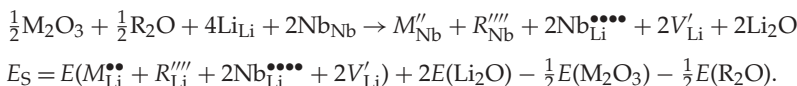
2. Self-compensation with $M = \text{Ce}^{3+}$, Fe^{3+} at a Li^+ site and $R = \text{Cu}^+$ at a Nb^{5+} site:



3. Substitution of $M = \text{Ce}^{3+}$, Fe^{3+} and $R = \text{Cu}^+$ at Nb^{5+} sites with Nb^{5+} anti-site compensation:



4. Substitution of $M = \text{Ce}^{3+}$, Fe^{3+} and $R = \text{Cu}^+$ at Nb^{5+} sites with charge compensation by a Nb^{5+} anti-site and a Li^+ vacancy:



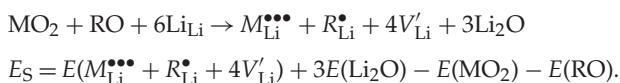
5. Substitution of $M = \text{Ce}^{3+}$, Fe^{3+} and $R = \text{Cu}^+$ at Nb^{5+} sites with charge compensation by an O^{2-} vacancy:



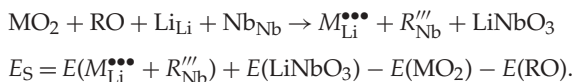
6. $E_S = E(M''_{\text{Nb}} + R''_{\text{Nb}} + 3V_{\text{O}}^{\bullet\bullet}) + E(\text{Nb}_2\text{O}_5) - \frac{1}{2}E(\text{M}_2\text{O}_3) - \frac{1}{2}E(\text{R}_2\text{O}).$

(c) One tetravalent and one divalent dopant ion ($M = \text{Ce}^{4+}$, $R = \text{Mn}^{2+}$)

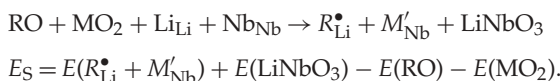
1. Substitution of $M = \text{Ce}^{4+}$ and $R = \text{Mn}^{2+}$ at Li^+ sites with Li^+ vacancy compensation:



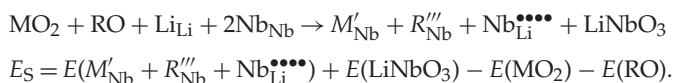
2. Self-compensation with $M = \text{Ce}^{4+}$ at a Li^+ site and $R = \text{Mn}^{2+}$ at a Nb^{5+} site:



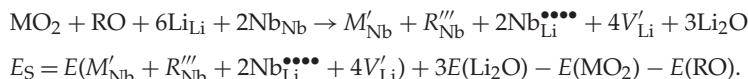
3. Self-compensation with $R = \text{Mn}^{2+}$ at a Li^+ site and $M = \text{Ce}^{4+}$ at a Nb^{5+} site:



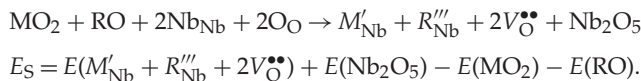
4. Substitution of $M = \text{Ce}^{4+}$ and $R = \text{Mn}^{2+}$ at Nb^{5+} sites with Nb^{5+} anti-site compensation:



5. Substitution of $M = \text{Ce}^{4+}$ and $R = \text{Mn}^{2+}$ at Nb^{5+} sites compensated by a Nb^{5+} anti-site and a Li^+ vacancy:

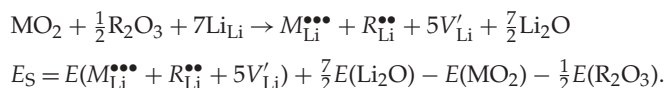


6. Substitution of $M = \text{Ce}^{4+}$ and $R = \text{Mn}^{2+}$ at Nb^{5+} sites with compensation by an O^{2-} vacancy:

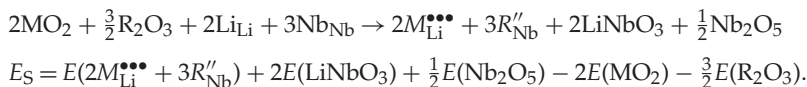


(d) One tetravalent and one trivalent dopant ($M = \text{Ru}^{4+}$, $R = \text{Fe}^{3+}$)

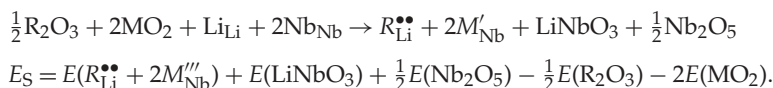
1. Substitution of $M = \text{Ru}^{4+}$ and $R = \text{Fe}^{3+}$ at Li^+ sites with Li^+ vacancy compensation:



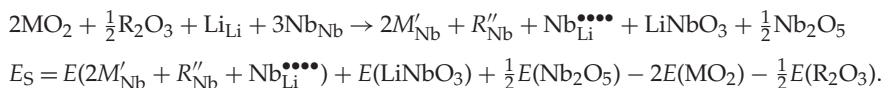
2. Self-compensation with $M = \text{Ru}^{4+}$ at a Li^+ site and $R = \text{Fe}^{3+}$ at a Nb^{5+} site:



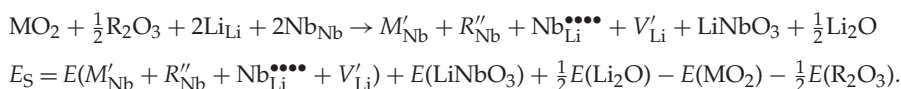
3. Self-compensation with $R = \text{Fe}^{3+}$ at a Li^+ site and $M = \text{Ru}^{4+}$ at a Nb^{5+} site:



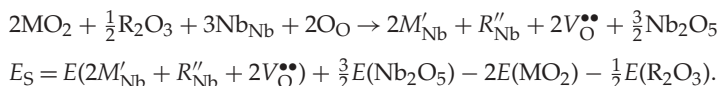
4. Substitution of $M = \text{Ru}^{4+}$ and $R = \text{Fe}^{3+}$ at Nb^{5+} sites with compensation given by a Nb^{5+} anti-site:



5. Substitution of $M = \text{Ru}^{4+}$ and $R = \text{Fe}^{3+}$ at Nb^{5+} sites with compensation given by a Nb^{5+} anti-site and Li^+ vacancy compensation:



6. Substitution $M = \text{Ru}^{4+}$ and $R = \text{Fe}^{3+}$ at Nb^{5+} sites with compensation given by an O^{2-} vacancy:



The solution energies were calculated for each of the above reactions using the expressions given. The basic defect formation energies and lattice energies required to calculate the solution energies are given in table 3. The defect formation energies and solution energies for each dopant combination are given in tables 4–7. The calculations were carried out assuming that the dopant and the charge-compensating defects are located at neighbouring sites, meaning that all formation energies include binding energies arising from the Coulombic interaction between the net charges of the defects.

In tables 4–7, the lowest solution energies for each pair of dopants are italicized. Comparing these results with available experimental data, it is noted that, for Ce^{4+} , Mn^{2+} doping (table 6),

Table 4. Defect formation energies and solution energies for Rh^{3+} , Fe^{3+} doping (see §3a).

	scheme (i)		scheme (ii)		scheme (iii)		scheme (iv)		scheme (v)		scheme (vi)	
	0	293	0	293	0	293	0	293	0	293	0	293
E_D (eV)	-41.86	-42.17	26.65	26.28	26.65	26.61	29.58	28.81	-32.95	-33.37	170.7	170.5
E_S (eV)	1.50	1.58	1.11	1.03	1.22	1.20	1.79	1.53	2.42	2.80	2.28	2.18

Table 5. Defect formation energies and solution energies for $\text{Ce}^{3+}/\text{Fe}^{3+}$, Cu^+ doping (see §3b).

	scheme (i)		scheme (ii)		scheme (iii)		scheme (iv)		scheme (v)		scheme (vi)	
	0	293	0	293	0	293	0	293	0	293	0	293
$\text{Ce}^{3+}\text{Cu}^+$												
E_D (eV)	-12.36	-12.85	56.64	56.64	57.95	57.32	-14.75	-15.60	189.4	189.3		
E_S (eV)	0.33	0.80	9.16	9.59	10.47	10.27	-2.07	-1.96	3.45	3.43		
$\text{Fe}^{3+}\text{Cu}^+$												
E_D (eV)	-11.36	-11.73	32.98	32.98	38.62	38.33	-25.59	-25.86	180.3	180.3		
E_S (eV)	12.44	13.15	7.73	8.40	13.37	13.75	-1.79	-0.98	3.39	3.28		

Table 6. Defect formation energies and solution energies for Ce^{4+} , Mn^{2+} doping (see §3c).

	scheme (i)		scheme (ii)		scheme (iii)		scheme (iv)		scheme (v)		scheme (vi)	
	0	293	0	293	0	293	0	293	0	293	0	293
E_D (eV)	-33.28	-33.61	25.78	25.78	26.78	26.45	39.52	39.17	-32.25	-32.96	178.3	170.5
E_S (eV)	3.53	3.45	-2.51	-2.73	-1.96	-2.98	-0.27	-0.33	34.29	31.33	3.61	3.56

Table 7. Defect formation energies and solution energies for Ru^{4+} , Fe^{3+} doping (see §3d).

	scheme (i)		scheme (ii)		scheme (iii)		scheme (iv)		scheme (v)		scheme (vi)	
	0	293	0	293	0	293	0	293	0	293	0	293
E_D (eV)	-38.26	-38.45	36.54	36.54	13.65	13.38	32.45	32.21	-33.19	-33.45	171.8	171.5
E_S (eV)	37.10	37.83	-11.18	-10.97	-11.05	-11.10	7.75	7.73	-32.93	-33.08	7.30	7.69

the calculations suggest scheme (iii) with occupation of both Li and Nb sites, which agrees with [21], which finds that the Ce^{4+} and Mn^{2+} ions occupy two sites with different site symmetries. For Ru^{4+} and Fe^{3+} (table 7), the two lowest energy schemes are highlighted, including scheme (ii), with the two ions substituting at both Li and Nb sites; this observation is consistent with the results of Xi *et al.* [22].

Looking at the solution energies in general, it is noted that, for the most favoured schemes in tables 5–7, they are negative. This is unusual compared with values obtained for single ion doping (which are usually positive), and implies that co-doping assists the doping process in these cases. For example, for the case of single Fe^{3+} doping [10], the most favourable mechanism involved incorporation of the dopant at both Li and Nb sites with solution energies of 0.16 eV at 0 K, and 0.94 eV at 293 K. Co-doping with either Ru^{4+} or Cu^+ results in negative solution energies, implying that doping is a favourable process. Similar results are observed for Ce^{3+} doping, where previous results [9] indicated that self-compensation at both Li and Nb sites was the most favourable mechanism, with solution energies of 0.85 eV and 1.25 eV for 0 K and 293 K, respectively. When Ce^{3+} is co-doped with Cu^+ , the lowest solution energies are

negative, indicating that it is easier to incorporate Ce^{3+} in the LiNbO_3 matrix when Cu^+ is also added.

4. Conclusion

The paper has presented a survey of doping of LiNbO_3 by transition metal ions, and predictions have been made of the energetically optimum sites for the location of these dopant ions. In addition, the predictions of the present study are in line with those of recent experimental work in this field.

Acknowledgements. M.E.G.V. is grateful to Conselho Nacional de Desenvolvimento Científico e Tecnológico (CNPq) for research support. This paper was submitted in honour of Professor Patrick Jacobs, who made so many important contributions to the field of solid-state chemistry.

References

- Jazbinsek M, Zgonik M. 2002 Material tensor parameters of LiNbO_3 relevant for electro- and elasto-optics. *Appl. Phys. B* **35**, 407–414. (doi:10.1007/s003400200818)
- Räuber A. 1978 Chemistry and physics of lithium niobate. In *Current topics in materials science 1* (ed. E Kaldis), p. 481. Amsterdam, The Netherlands: North-Holland.
- Prokhorov AM, Kuzminov YS. 1990 *Physics and chemistry of crystalline lithium niobate*. New York, NY: Hilger.
- Wong KK (ed.). 2004 *Properties of lithium niobate*. Piscataway, NJ: IEE.
- Li D, Liu D, Zhi Y, Luan Z, Liu L. 2009 Study of near-infrared nonvolatile two-centre holographic recording in $\text{LiNbO}_3\text{:Fe:Rh}$ crystal. *Optik* **120**, 313–317. (doi:10.1016/j.ijleo.2007.09.006)
- Zhen XH, Li HT, Sun ZJ, Ye SJ, Zhao LC, Xu YH. 2004 Holographic properties of double-doped Zn:Fe:LiNbO_3 crystals. *Mater. Lett.* **58**, 1000–1002. (doi:10.1016/j.matlet.2003.08.005)
- McMillen DK, Hudson TD, Wagner J, Singleton J. 1998 Holographic recording in specially doped lithium niobate crystals. *Opt. Express.* **2**, 491–502. (doi:10.1364/OE.2.000491)
- Jackson RA, Valerio MEG. 2005 A new interatomic potential for the ferroelectric and paraelectric phases of LiNbO_3 . *J. Phys. Condensed Matter* **17**, 837–843. (doi:10.1088/0953-8984/17/6/005)
- Araujo RM, Lengyel K, Jackson RA, Kovács L, Valerio MEG. 2007 A computational study of intrinsic and extrinsic defects in LiNbO_3 . *J. Phys. Condensed Matter* **19**, 046211. (doi:10.1088/0953-8984/19/4/046211)
- Araujo RM, Valerio MEG, Jackson RA. 2008 Computer modelling of trivalent metal dopants in lithium niobate. *J. Phys. Condensed Matter* **20**, 035201. (doi:10.1088/0953-8984/20/03/035201)
- Mott NF, Littleton MJ. 1938 Conduction in polar crystals. I. Electrolyte conduction in solid salts. *Trans. Faraday Soc.* **34**, 485–499. (doi:10.1039/tf9383400485)
- Gale JD. 1997 GULP: a computer program for the symmetry-adapted simulation of solids. *J. Chem. Soc. Faraday Trans.* **93**, 629–637. (doi:10.1039/a606455h)
- Ben-Dor L, Fischbein E, Kalman Z. 1976 Concerning the β phase of iron (III) oxide. *Acta Crystallogr. B* **32**, 667. (doi:10.1107/S0567740876003749)
- Malecka MA, Kepinski L, Maczka M. 2008 Structure and phase composition of nanocrystalline $\text{Ce}_{1-x}\text{Lu}_x\text{O}_{2-y}$. *J. Solid State Chem.* **181**, 2306–2312. (doi:10.1016/j.jssc.2008.05.033)
- Hirosaki N, Ogata S, Kocer C. 2003 Ab initio calculation of the crystal structure of the lanthanide Ln(2)O(3) sesquioxides. *J. Alloys Compd.* **351**, 31–34. (doi:10.1016/S0925-8388(02)01043-5)
- Kirfel A, Eichhorn KD. 1990 Accurate structure-analysis with synchrotron radiation: the electron density in Al_2O_3 and Cu_2O . *Acta Crystallogr. A* **46**, 271–284. (doi:10.1107/S0108767389012596)
- Trukhanov SV, Troyanchuk IO, Bobrikov IA, Simkin VG, Balagurov AM. 2007 Crystal structure phase separation in anion-deficient $\text{La}_{0.70}\text{Sr}_{0.30}\text{MnO}_{3-s}$ manganite system. *J. Surface Invest. X-ray, Synchrotron Neutron Tech.* **1**, 705–710. (doi:10.1134/S1027451007060158)
- Poepfelmeier KR, Ansell GB. 1981 Growth of the high temperature, high pressure polymorph of Rh_2O_3 by chemical-transport with HCl. *J. Crystallogr. Growth* **51**, 587–588. (doi:10.1016/0022-0248(81)90441-3)

19. Foo ML, Huang Q, Lynn JW, Lee WL, Klimczuk T, Hagemann IS, Ong NP, Cava RJ. 2006 Synthesis, structure and physical properties of Ru ferrites: $\text{BaMRu}_5\text{O}_{11}$ ($M = \text{Li} \ \& \ \text{Cu}$) and $\text{BaM}'_2\text{Ru}_4\text{O}_{11}$ ($M' = \text{Mn}, \text{Fe} \ \& \ \text{Co}$). *J. Solid State Chem.* **179**, 563–572. (doi:10.1016/j.jssc.2005.11.014)
20. Kröger FA, Vink HJ. 1954 The origin of the fluorescence in self-activated ZnS, CdS, and ZnO. *J. Chem. Phys.* **22**, 250.
21. Wang M, Wang R, Li C-Y, Xu Y-L, Wang J, Liu W-H, Yang C-H. 2008 Optical properties of Ce: Mn: LiNbO_3 crystals with various [Li]/[Nb] ratios. *J. Crystallogr. Growth* **310**, 3820–3824. (doi:10.1016/j.jcrysgr.2008.05.029)
22. Xi Q, Liu D, Zhi Y, Luan Z, Liu L. 2005 Reversible electrochromic effect accompanying domain-inversion in $\text{LiNbO}_3\text{:Ru:Fe}$ crystals. *Appl. Phys. Lett.* **87**, 121103. (doi:10.1063/1.2053356)